Measuring the size of oil droplets in a flow cytometer using Mie resonances-a possible size calibration ladder for 0.5 μm to 6 μm

Richard E. Cavicchi*, Dean C. Ripple†, Joshua A. Welsh[#], Jerilyn R. Izac*, Alexander W. Peterson*, Aaron M. Goldfain[$], Wyatt N. Vreeland*

*Materials Measurements Laboratory, National Institute of Standards and Technology, Gaithersburg, Maryland 20899

†Materials Measurements Laboratory, National Institute of Standards and Technology, Gaithersburg, Maryland 20899 (Retired)

[#]Laboratory of Pathology, Translational Nanobiology Section, Centre for Cancer Research, National Institute of Health, National Institutes of Health, Bethesda, MD, USA and Advanced Technology Group, Becton Dickinson, San Jose, California, USA

[$]Sensor Science Division, Physicial Measurements Laboratory, National Institute of Standards and Technology, Gaithersburg, Maryland 20899

Correspondence: R.E. Cavicchi, Materials Measurements Laboratory, National Institute of Standards and Technology, Gaithersburg, Maryland 20899

Email: Richard.Cavicchi@nist.gov

ABSTRACT

An emulsion of silicone oil droplets in aqueous buffer produces a distinctive series of peaks or resonances in the side scatter histogram in a flow cytometer. As many as 12 peaks are observed in the violet-side scatter channel at 405 nm, with half that number observed in the blue side scatter channel at 488 nm. Using the index of refraction of the oil and buffer, the wavelength of light, and the collection angle and gain of the instrument, we assign the peaks to specific diameters at which Mie resonances occur. With the close match for the index of refraction of silicone oil (n=1.417 at 405 nm) to biological materials, these resonances could form the basis of a finely spaced size calibration ladder in the range 0.5 μm to 6 μm for estimating the size of biological particles in a flow cytometer. Resonances were also observed using mineral oil (n=1.483 at 405 nm) suggesting that investigating and modeling resonances for emulsion systems may be useful for understanding these systems.

INTRODUCTION

Light scattering from particles passing through a flow cytometer produce signals that depend upon a particle's size, as well as other factors such as shape, index of refraction n, and 'granularity'. This enables the counting of particles paired with each particle's scattering intensity to produce a distribution of count vs intensity, which can be useful for characterizing a mixed population of particles. For biological samples, the signal from light obscuration, the method most commonly used to assess particles in the range 2 μm to 100 μm in the biopharmaceutical industry, is also directly related to light scattering. Both methods can be traced back to an early concept described by Moldavan in 1934. [1] The continued discovery of new uses for flow cytometry (FC) has been accompanied by advances in instrumentation, including more sensitive detection, and a variety of sources and filters for fluorescence detection. There

has been interest in applying these instruments with their wide dynamic range in counts and size, for measuring size distributions for a variety of biological particles, including cells and protein aggregates [2 3 4 5 6 7], as well as for submicrometer particles such as extracellular vesicles. [8 9 10 11] Quantitatively establishing accurate particle size of biological samples remains a challenge for these new applications.

It is common to use size-calibrated microspheres for instrument performance checks and also to provide an estimate for size in a measurement. Light scattering from microspheres is described by the Mie model{Nieto-Vesperinas, 2020 #747}. It has been understood from Mie model calculations that the difference in index of refraction between the calibration microspheres and the particles of interest will lead to differences between the calibration microsphere size and the test sample particle size, for the same detected signal levels. Larger differences in refractive index between the particle and the surrounding medium (often water or buffer with n=1.33) result in a larger scattering signal. Examples from literature for widely available polystyrene latex (PSL) with n=1.6 include the following: Polymeric microbeads 5 μm in diameter, appear to have the same forward scatter (FSC) signal as lymphocytes which are 8 μm in diameter;[12] A polystyrene microsphere 0.4 μm in diameter produced the same FSC intensity as a 1 μm lipid or cellular microparticle; [13] Side scatter (SSC) intensity from 110 nm polystyrene beads corresponded to the scattering from ≈400 nm vesicle-like particles.[14] These examples are specific for the optical configuration (collection angles, wavelength) of the involved flow cytometers. Biological particles have values of n much closer to the value of water (and most buffer solutions). Typical values for n for biological particles are n=1.36 to 1.40 for bacteria, [15] n=1.37 to 1.42 for red blood cells,[16] average values of n=1.38 for liver cells, [17] n=1.37 for platelets, [13] n=1.34 to 1.40 for protein aggregates, [18,19] and n=1.37 to 1.39 for extracellular vesicles.[9 10 20]

Alternatives to PSL microspheres as reference particles have been used that have a closer index of refraction match to biological particles. A common choice has been silica microspheres. Although the index of refraction of bulk fused silica is n=1.463 at 500 nm wavelength[21 22] silica in microsphere form has a reported index used to analyze data from n=1.42 to n=1.46. [15 13 23 10 24 25 11 26] The decrease from the bulk value is likely resulting from porosity [23], which may depend on the manufacturing process or batch.[27] Other options for calibration microspheres such as hollow organosilica beads, which have core-shell properties similar to extracellular vesicles,[28] hydrogel beads,[29] and extruded liposomes[14] have been proposed. These materials require custom fabrication and analysis prior to use as standards. In this paper, we explore the use of suspensions of silicone or mineral oil droplets, which are readily prepared and which have a consistent and predictable refractive index.

To make the best use of calibration microspheres, it is important to account for the instrument scattering geometry. Welsh et al. have reported on a method and developed a software tool designed for submicrometer particle analysis called FCM_{PASS} that uses measurements on a set of microspheres to generate a value for the instrument's SSC collection angle, as well as providing scatter-diameter curves and scatter-refractive index curves that can be used for data analysis.[26] The collection angle is an essential parameter, which can vary for instruments from different manufacturers, and also between instruments of the same model type due to variations on the optical alignment.

In 1908, Gustav Mie used Maxwell's equations to develop a solution to the scattering and absorption of light by a small absorbing sphere and applied the results to gold colloids. [30] A feature of the solution is a series of peaks or 'resonances' that will be observed in the intensity vs. scattering angle or particle diameter.[26,31] The calibration process described by van der Pol et al. [9] and Welsh et al [26] fits average

values for each diameter value to a Mie calculation that includes effects of the resonances. Mie peaks have been measured as a function of forward scattering angle in a custom instrument using PSL microspheres.[32] "Lissajous-like" patterns in SSC Vs FSC dot plots were observed by Doornbos et al. in a custom flow cytometer. [33] The features in that work were observed from nominally monodisperse PSL microspheres of 2.23 μm and 7.04 μm and were correlated to Mie scattering calculations based on a Gaussian dispersion in size for each nominal size value. Satinover et al. compared light obscuration with flow cytometry for lipid-coated microbubbles. [34] In flow cytometry they observed a serpentine structure in the SSC vs FSC scatter plot consistent with Lorenz-Mie calculations. The fit to model was used for sizing the microbubbles. Fattaccioli et al. characterized emulsions of soybean oil and observed a serpentine structure in in the SSC vs FSC scatter plot which agreed with models from Mie theory.[35]

We report here a striking series of peaks in Violet Side Scatter (VSSC) and SSC from silicone oil and mineral oil droplets in buffer solution. Using a Mie scattering model, we are able to assign the peaks to diameter values of the droplets. Key to using the model is knowledge of the collection angle of the cytometer, for which we use the method of Welsh et al.[26,36] Silicone oil has a refractive index close to biological materials and thus these peaks can be used as a means of obtaining the size of biological particles in the (0.5 to 6) μm diameter range.

MATERIALS AND METHODS

Sample Preparation

For calibration of the instrument's collection angle, we used polystyrene size standards Thermo Fisher Scientific, 3000 series –3080A, 3100A, 3150A, 3200A, 3200A, 3269A, 3300A, 3350A, 3400A, 3450A, 3500A, 3600A, corresponding to diameters (80, 100, 150, 200, 240, 270, 300, 350, 400, 450, 500, and 600) nm[37]. Silica microspheres with reported diameters 0.4 μm, 0.5 μm, and 1.2 μm were obtained from nanoComposix (San Diego, CA), 3.62 μm and 4.08 μm from Cospheric LLC (Santa Barbara, CA,) and 2.56 μm, 3.6 μm, and 6.10 μm were obtained from Bangs Laboratories (Fishers, IN).

Suspensions of silicone oil droplets were prepared following the recipe of Vandesteeg and Kilbert. [38] Briefly, polydimethylsiloxane (Brookfield Ametek, Middleboro, MA) at a mass fraction of 0.1 % was added to a buffer consisting of 10 mmol/L phosphate buffer (pH 7.4), 150 mmol/L NaCl, and 0.02 % mass fraction polysorbate 20. The mixture was sonicated for 15 min. Suspensions of mineral oil droplets (from NIST SRM 1922 [39]) were prepared using the same procedure. It is expected that this process produces a broad range of oil droplet sizes. [38 40] For one experiment, silicone oil droplets were labeled with BODIPY 493/503, (Thermo-Fisher/Invitrogen Waltham, MA). BODIPY powder was dissolved in dimethyl sulfoxide at 2.5 mg/mL. This was added to the silicone oil droplet solution at 1 μL/mL. Index values were reported at 20 °C.

Measurement of Silicone Oil index of refraction

Refractive index measurements were performed on a home-built critical angle refractometer. [41] The instrument design is based on a prism-coupled surface plasmon resonance sensor with angular modulation used here without a metal layer[42,43]. The optical setup focuses and collects a wedge of light, with angle width of ≈10^{o}, allowing for a simultaneous collection of the angular span of incident light. Individual LED light sources (625 nm, 590 nm, 505 nm, Thorlabs; 515 nm, WT&T Inc., 455 nm, 415 nm, 340 nm, Mightex) were sequentially coupled through a multimode fiber optical cable, collimating lens,

rectangular slit, and then focused with a hemicylindrical lens towards a mounted hemicylindrical BK7 glass prism assembly. A BK7 glass slide was optically coupled to the prism with index match fluid (n=1.515, Cargille) and a Teflon fluid chamber cell was fixed to the slide/prism assembly. The reflected wedge of light was directly detected with a 3000-pixel linear CCD camera (Thorlabs). The detected angle range was adjusted to capture the critical angle for all samples collected ≈ 60° to 70° incident.

Sample solutions were injected into a measurement chamber after thorough rinsing for each sample. At the start of an experiment a reflectance curve was taken at each wavelength in air. A reflectance curve was then taken at each wavelength for each sample solution. After the experiment a normalized reflectance curve was generated by dividing the sample solution reflectance curve by the air reflectance curve at each measured wavelength. Reflectance curves were obtained for calibration solutions: water (18 MΩ·cm, Millipore), methanol, ethanol, and butanol (HPLC grade, Sigma-Aldrich) followed by the silicone oil sample at each wavelength. The experiment was repeated three times. Measurements were made at a temperature of 21 °C.

All data fitting were performed using custom and stock code written in MATLAB and MATLAB Optimization toolbox. The critical angle reflectance curves were analyzed by fitting the data to a 2-layer Fresnel model[44] using published relations for the prism[45], and the calibration solutions[46-48]. The calibration solutions were used to obtain the pixel-to-angle conversion. The fitted variable was the refractive index of the silicone oil sample performed at each wavelength. A refractive index versus wavelength plot was generated (Supplemental Figure 1) with standard deviation for three experimental repeats and fit to a 3-term Cauchy equation, $n = A + B/\lambda^2 + C/\lambda^4$, with the coefficients: A = 1.3913, B = 3070 nm^2, C = 1.848× 10^8 nm^4 [49]. From this dispersion relation, a refractive index 1.4168 for 405 nm and 1.4074 for 488 nm was used in subsequent Mie calculations for the silicone oil. The standard uncertainty in the refractive index is estimated as 0.0005, which accounts for the variation among repeated experiments and the residuals from the fit to the Cauchy equation.

Flow Cytometer Configuration

A Beckman Coulter CytoFLEX LX, which included lasers of 80 mW at 405 nm and 50 mW at 488 nm was used for most studies. This instrument features a violet side scatter (VSSC) detection mode, using the 405 nm laser which combined with its detector enables detection of smaller particles than can be detected by 488 nm side scatter (SSC).[11] For additional information on cytometer settings see attached MIFlowCyt (Supplementary Table 1). Analysis was done using signal height. The threshold for detection was set using the VSSC channel at a value of 1400, at which the noise signal is just evident in the histogram of pure water (Supplementary Figure 2.) All data was collected using the VSSC channel as trigger. The FSC and SSC channels show a clear noise peak under these conditions for low scattering intensity (see Supplementary Figure 2.) An Attune NxT was used to demonstrate the Mie resonances on a separate FC, with settings supplied also in the attached MIFlowCyt (Supplementary Table 1).

Collection Angle Determination

The instrument collection angle *a* is a key parameter in the analysis of Mie scattering data. It is not generally provided with instrument information and can depend on optical alignment. We used the method of Welsh et al. to determine *a*.[26,36] Briefly, histograms were collected for a set of polystyrene microspheres with diameters 81 nm to 600 nm and the results of peak intensities provided to the software tool FCM$_{PASS}$. The results are shown in Supplementary Figures 3 and 4. The fit to Mie theory

gave a collection half-angle of 56.0° for the Cytoflex, and 48.8° for the Attune NxT. Values for Cytoflex model S of 53.2°, [50] 54.1°, [51] and 55° [52] have been reported.

Intensity Units for Side Scattering

FCM_{PASS} also provides a multiplication factor for converting side scatter intensities to standard cross section units (SCS) (nm^2). We used these factors for VSSC and SSC (0.01182 and 1.263 respectively for Cytoflex) and SSC (0.6265 for Attune) in SCS units (nm^2) to convert instrument scattering intensity to SCS units for our plots. Forward scattering (FSC) intensity was left in the arbitrary units reported by the instrument.

Data Analysis

Calculations of scattering intensity versus diameter using Mie theory were done using MiePlot.[53] The software takes as inputs the wavelength, index of refraction of the medium and sphere, collection angle, angle step size, and diameter step size. Table 1 shows the index of refraction values that were used for the silicone and mineral oils (spheres), as well as for the PBS buffer (medium).[39,54] MiePlot calculated intensity was scaled to Cytoflex LX intensity using the ratio of intensity values for 1.2 μm silica microspheres at 405 nm with n=1.46. This gain was 1.09×10^{18}.

Files were converted from FCS format to CSV format using the FlowCore software package for the R programming language https://bioconductor.org/packages/release/bioc/html/flowCore.html Histograms were based on the log of the scattering intensity with bin size equal to 0.025. Moving average for dot plots was created by sorting the data by VSSC value, and computing the average value of the VSSC intensity in each bin, as well as the average of the corresponding FSC and SSC values for particles in that bin.

RESULTS and DISCUSSION

Histograms of VSSC intensities from silicone oil droplets and mineral oil droplets are shown in Figure 1. Both samples showed a striking series of peaks which have the largest spacing and amplitude at the lowest scattering intensity. The silicone oil droplet peak series was shifted to lower intensity compared to the mineral oil peak series, and also had narrower spacing between the peaks. VSSC histograms from three runs spanning four months show that the peak locations are at the same VSSC values (Supplementary Figure 5.) Dilution of samples did not change the locations of the peaks (Supplementary Figure 6.)

The data were suggestive of a Mie scattering resonance phenomena occurring in the scattering of light by the size-distributed oil droplets. Figure 2 shows a calculation of the Mie scattering for spheres of index 1.417 as a function of diameter obtained using MiePlot. The calculated scattering increases with increasing diameter, and, beginning at close to 0.5 μm, is modulated by a series of plateaus. Taking the derivative of this curve with respect to diameter reveals the structure in greater detail. The minima are approximately equally spaced in diameter, with a period of approximately 0.5 μm. A second way of understanding the peaks is shown in the Supplementary Figure 7, which shows a polar plot of scattering intensity vs scattering angle for three values of particle radius. As the radius of the sphere increases, an additional lobe is included in the collection angle. As the radius continues to increase, the inclusion of these lobes gives rise to the periodic structure of scattering vs diameter.

The size distribution of similarly prepared oil droplets has been shown to rise exponentially with decreasing size and is without peaks [38]. The appearance of features in the VSSC histogram is assigned to

the 'piling up' of particles where the scattering value does not change appreciably with change in particle diameter, at certain scattering values indicated by the plateaus in Figure 2. Taking the derivative with respect to diameter plotted against diameter (Figure 2, dashed curve) results in a series of sharp minima corresponding to the plateaus. The inverse of the derivative shown in Figure 2, is the derivative of the diameter with respect to scattering intensity, d(Diameter)/d(Scaled VSSC) which can be plotted as a function of the scattering intensity. Here, "Scaled VSSC" references that the scattering intensity has been scaled from the calculation to the instrument scattering intensity using the scaling factor as described in the Data Analysis section. Figure 3 (A) shows the VSSC data histogram for silicone oil (solid blue curve), together with d(Diameter)/d(Scaled VSSC) (dashed red curve). There is good correlation between the observed peaks and the calculated resonances, especially for the peaks at lower scattering intensity (smaller particles). The effect of index of refraction used for silicone oil and collection angle used for the Mie scattering calculations is shown in Supplementary Figure 8. Supplementary Figure 8A) shows small differences in index of refraction can affect the fit, with a value of n=1.420 giving an improved fit for larger particles. We note that n for silicone oil was measured at 21 °C, while the temperature inside the spectrometer was not measured (ambient was measured at 19 °C), such small differences in temperature can produce small changes in the index of refraction[41]. The diameter corresponding to the Mie peaks, however, depends only weakly on n. Similarly, the diameter associated with peaks depends weakly on the collection angle (Supplementary Figure 8(B). Assignment of a diameter to the experimental peaks is possible to within two percent. Sources of error are discussed further below in connection with Figure 7.

Figure 3(B) shows the corresponding plot of Figure 3(A) for mineral oil with index n=1.483. This results in peaks at higher scattering values, but similar diameter values. The calculation for n=1.483 also reveals a finer structure of oscillation, which obscures the discernment of the broad peaks at diameter values above 3 μm. For further illustration of this point, see the polar plot in Supplementary Figure 9.

The observation of peaks in the histograms for oil droplets is not limited to detection at 405 nm. Figure 3(C) shows the observed peaks detected in the SSC channel at 488 nm (solid blue curve) for silicone oil. The Mie calculation for the derivative d(Diameter)/d(Mie Scattering signal) for silicone oil at n=1.407 and 488 nm is shown in red. The spacing between the peaks in diameter is approximately 0.6 μm. Figure 3(C) also shows the results from an Attune NxT flow cytometer, showing the Mie scattering phenomenon may be useful to other spectrometers than the Cytoflex.

Extracting the value of the scattered intensity at each of the peaks (silicone oil Figure 3(A) and mineral oil Figure 3(B)) along with the corresponding diameter assignment from the Mie calculation produces the results shown in Figure 4(A) for silicone oil (purple squares) and mineral oil (gray triangles). Also, included as an example comparison in this figure are the data for silica microspheres (yellow circles). The oil results appear smoother or less noisy than the silica, possibly due to variations in refractive index of silica spheres from different suppliers. For the histogram bin corresponding to the VSSC peak values, we also extract the mean FSC and SSC scattering values for those same particles. Figure 4 (B) and 4 (C) show the results that correspond to Figure 4 (A) for SSC and FSC channels. The FSC channel shows less sensitivity of the diameter dependence of scattering signal on index of refraction, compared to the side-scatter data. Both the SSC and FSC results do not show information from the 0.5 μm resonance seen in the VSSC channel as the corresponding SSC and FSC scattering intensities lie below the noise threshold for those channels (see Supplementary Figure 2.) The SSC and FSC channels detect only 17% and 13%,

respectively of the particles detected above the noise threshold in the VSSC channel, missing the small particles detected in VSSC, as shown in Supplementary Figure 10.

It is possible to use only the SSC channel, via the data of Figure 3(C) to obtain analogous results to Figure 4 relating diameter to SSC and FSC intensities. This simulates instruments that do not have the VSSC channel. Figure 5 compares the results for SSC and FSC using the VSSC channel calibration from Figure 3 (A) (blue squares) with the results using the SSC channel calibration from Figure 3 (C) (black triangles).

Results from the VSSC calibration using silicone oil droplets for the three channels are combined in Figure 6. This shows how a droplet diameter may be estimated based on the scattering signals. Vertical error bars appearing on some of the VSSC data points (for some, the error bars are smaller than the symbol) represent the spread in diameter assignments as illustrated in Supplementary Figure 8 due to possible error in *n* or collection angle. Uncertainty in the scattering signal for VSSC data points from the standard deviation from measurements made at different dates (Supplementary Figure 5) ranged from one to four percent of the scattering signal value and were smaller than the size of the data points. Error bars on the SSC and FSC data in Figure 6 represent the standard deviation in SSC and FSC values obtained from VSSC data points that have a scattering signal within two percent of the plotted VSSC points. This represents expected scatter in FSC and SSC among individual points, and includes effects of the higher noise in those channels. The data points themselves for SSC and FSC represent the mean value, for which an error bar would be the standard error of the mean, which is less than one percent of the scattering value and smaller than the data points.

As a final test of this approach, we prepared a sample of silicone oil droplets, where the oil droplets were labeled with BODIPY dye. Addition of dye generated some particles which from the SSC-VSSC dot plots were not silicone oil droplets. A polygon gate was used to remove those particles (Supplementary Figure 11.) Figure 7 shows a comparison of the histograms of the unstained and BODIPY-labeled silicone oil droplets. The location of the peaks appears unaffected by the addition of the stain. For each peak, the corresponding Mie diameter was obtained as in Figure 3 (A), and the corresponding fluorescence intensity was recorded. The inset shows the BODIPY fluorescence intensity vs diameter for these peaks. The line indicates a dependence on the cube of the diameter, showing that the results are consistent with the oil-droplets being bulk-labeled, and that the assigned peak diameters are consistent with the fluorescence results from bulk-labeled droplets.

Application of the results here for silicone oil to biological materials could be implemented by obtaining an estimate of *n* for the biological particles. Supplementary Figure 8A provides an example of how the calculated scattering intensity for the Mie peak depends on *n*, and thus gives an indication of the expected shifts as the *n* of biological particles differs from that of silicone oil. Note that the appropriate *n* here is that at wavelength 405 nm. Using the estimate for *n*, one may calculate the expected shift in scattering intensity of droplets with that *n* relative to silicone oil. This would provide points along the scattering intensity axis that could then be converted using the silicone oil calibration to give an estimated diameter. Uncertainty in the results would likely be dominated by the uncertainty of the index of refraction of the particles being tested. Also differences between the estimated diameter and actual particle size will likely arise due to particle shape, and internal inhomogeneity and porosity. An alternative approach is to use the values for FSC to estimate size using the results in Figure 7, since FSC is less strongly dependent on these properties.

CONCLUSION

Flow cytometry measurements of side-scattering histograms from an emulsion of oil droplets in aqueous buffer show a series of peaks that are distinct from histograms resulting from other particle samples reported using this method. These peaks are manifestations of Mie Scattering. While more peaks are observed at 405 nm (VSSC), the effect is prominent at 488 nm (SSC). Using the index of refraction of the oil and buffer, the wavelength of light, and the collection angle and gain of the instrument, it is possible to assign the peaks to specific diameters at which Mie resonances occur. At 405 nm, silicone oil droplets with n=1.417 give rise to resonances spaced by 0.5 μm, starting at 0.5 μm. The refractive index value of silicone oil matches more closely with biological materials, compared to calibration microspheres of polystyrene or silica, and the series of closely spaced peaks could serve as a calibration ladder for the size range 0.5 μm to 6 μm. These peaks would provide a reference point for checking any models based on Mie scattering for test particles, which, without the nearly perfect sphericity of the oil droplets, would not produce resonances. Without the resonances, factors such as particle shape or internal structure can make it difficult for a Mie model to estimate size. The appearance of these resonances may be of interest in the study of emulsions, where, for example, modeling of droplets with core-shell structure may be of interest.

ACKNOWLEDGEMENT

We are grateful to Sandra Da Silva, Kirsten Parratt, and Nancy Lin of the Biomaterials Group, NIST, for the use of their flow cytometer, and for fruitful discussions and problem-solving in obtaining measurements.

	488 nm	405 nm
PBS buffer	1. 337	1. 343
Silicone Oil	1.407	1.417
Mineral Oil	1.475	1.483

Table 1. Index of refraction of buffer, silicone oil, and mineral oil used in Mie Models.

FIGURE CAPTIONS

Figure 1. Histogram of droplets detected at 405 nm (VSSC) for samples containing silicone oil droplets (solid blue line) and mineral oil droplets (dashed line).

Figure 2. Calculated (using Mieplot) scattering intensity vs diameter for a sphere with n=1.417 in water (solid black, left-axis) and the derivative (d(Mie Scattering signal)/d(Diameter) (dashed blue, right-axis). Approximate period is 0.5 mm.

Figure 3. (A) Histogram of particles detected at 405 nm (VSSC) for samples containing silicone oil droplets (solid blue line, left axis) and the derivative vs VSSC d(Diameter)/d(Mie Scattering signal) (dashed red line, right axis), where the calculated scattering intensity is scaled using results from 1.2 mm silica microspheres. Diameters indicated by the arrows come from the corresponding diameter from the

Mie calculation. (B) Histogram of particles detected at 405 nm (VSSC) for samples containing mineral oil droplets (solid blue line, left axis) and the derivative d(Diameter)/d(Mie Scattering signal) vs VSSC (dashed red line, right axis). (C) Histogram of particles detected at 488 nm (SSC) for samples containing silicone oil droplets (solid line, left axis) and the derivative vs SSC d(Diameter)/d(Mie Scattering signal) (dashed line, right axis). Blue curves correspond to results and modeling for Cytoflex instrument, and Orange for the Attune NXT. Modeling data for the latter is scaled by 0.01 for clarity. For the Cytoflex, approximate period is 0.6 mm, contrasting with the period 0.5 mm for the data at 405 nm (A).

Figure 4. Scattering intensity vs particle diameter for droplets of silicone oil (purple squares) and mineral oil (gray triangles) in water and silica microspheres for (A) VSSC, (B) SSC, and (C) FSC.

Figure 5. Comparison of silicone oil droplet results where calibration was performed using the VSSC data (blue squares) and SSC data (black triangles) for (A) SSC and (B) FSC.

Figure 6. Silicone oil droplet diameter vs scattering signal for VSSC (orange squares), SSC (blue diamonds), and FSC (gray triangles). Vertical error bars appearing on some of the VSSC data points (for some, the error bars are smaller than the symbol) represent the spread in diameter assignments as illustrated in Supplementary Figure 8 due to possible error in *n* or collection angle. Uncertainty in the scattering signal for VSSC data points from the standard deviation from measurements made at different dates (Supplementary Figure 5) ranged from one to four percent of the scattering signal value and were smaller than the size of the data points. Error bars on the SSC and FSC represent the standard deviation in SSC and FSC values obtained from VSSC data points that have a scattering signal within two percent of the plotted VSSC points. This represents expected scatter in FSC and SSC among individual points and includes effects of the higher noise in those channels. The data points themselves for SSC and FSC represent the mean value, for which an error bar would be the standard error of the mean, which is less than one percent of the scattering value and smaller than the data points. Scattering signal is in SCS units (nm^2) for VSSC and SSC, and in the arbitrary units reported by the instrument for FSC.

Figure 7. BODIPY-stained silicone oil droplets (solid orange line) and unstained droplets (dashed blue line). Inset: Bodipy fluorescence signal vs silicone oil droplet diameter as calibrated by Mie resonance, (purple diamond), and fit of fluorescence signal to the cube of the diameter.

REFERENCES

1. Moldavan A 1934. Photo-Electric Technique for the Counting of Microscopical Cells. Science 80(2069):188-189.
2. Ludwig DB, Trotter JT, Gabrielson JP, Carpenter JF, Randolph TW 2011. Flow cytometry: A promising technique for the study of silicone oil-induced particulate formation in protein formulations. Anal Biochem 410(2):191-199.
3. Nishi H, Mathas R, Furst R, Winter G 2014. Label-Free Flow Cytometry Analysis of Subvisible Aggregates in Liquid IgG1 Antibody Formulations. J Pharm Sci 103(1):90-99.
4. Lubich C, Malisauskas M, Prenninger T, Wurz T, Matthiessen P, Turecek PL, Scheiflinger F, Reipert BM 2015. A Flow-Cytometry-Based Approach to Facilitate Quantification, Size Estimation and Characterization of Sub-visible Particles in Protein Solutions. Pharm Res 32(9):2863-2876.

5. indexHu ZS, Ye C, Mi W, Zhao Y, Quan C, Li WW, Li HM, Hang HY 2018. Light-scattering detection within the difficult size range of protein particle measurement using flow cytometry. Nanoscale 10(41):19277-19285.
6. Probst C 2020. Characterization of Protein Aggregates, Silicone Oil Droplets, and Protein-Silicone Interactions Using Imaging Flow Cytometry. J Pharm Sci 109(1):364-374.
7. Hu Z, Mi W, Ye C, Zhao Y, Cavicchi RE, Hang H, Li H 2023. Global Analysis of Aggregation Profiles of Three Kinds of Immuno-Oncology mAb Drug Products Using Flow Cytometry. Anal Chem 95(10):4768-4775.
8. van der Pol E, Hoekstra AG, Sturk A, Otto C, van Leeuwen TG, Nieuwland R 2010. Optical and non-optical methods for detection and characterization of microparticles and exosomes. J Thromb Haemost 8(12):2596-2607.
9. van der Pol E, Coumans FA, Grootemaat AE, Gardiner C, Sargent IL, Harrison P, Sturk A, van Leeuwen TG, Nieuwland R 2014. Particle size distribution of exosomes and microvesicles determined by transmission electron microscopy, flow cytometry, nanoparticle tracking analysis, and resistive pulse sensing. J Thromb Haemost 12(7):1182-1192.
10. Nolan JP 2015. Flow Cytometry of Extracellular Vesicles: Potential, Pitfalls, and Prospects. Current Protocols in Cytometry 73(1):13.14.11-13.14.16.
11. Brittain GIV, Chen YQ, Martinez E, Tang VA, Renner TM, Langlois MA, Gulnik S 2019. A Novel Semiconductor-Based Flow Cytometer with Enhanced Light-Scatter Sensitivity for the Analysis of Biological Nanoparticles. Sci Rep-Uk 9.
12. Schwartz A, Fernandezrepollet E 1994. Standardization for Flow-Cytometry. Method Cell Biol 42:605-626.
13. Chandler WL, Yeung W, Tait JF 2011. A new microparticle size calibration standard for use in measuring smaller microparticles using a new flow cytometer. Journal of Thrombosis and Haemostasis 9(6):1216-1224.
14. Simonsen JB 2016. A liposome-based size calibration method for measuring microvesicles by flow cytometry. J Thromb Haemost 14(1):186-190.
15. Foladori P, Quaranta A, Ziglio G 2008. Use of silica microspheres having refractive index similar to bacteria for conversion of flow cytometric forward light scatter into biovolume. Water Res 42(14):3757-3766.
16. Zhang QN, Zhong LY, Tang P, Yuan YJ, Liu SD, Tian JD, Lu XX 2017. Quantitative refractive index distribution of single cell by combining phase-shifting interferometry and AFM imaging. Sci Rep-Uk 7.
17. Beuthan J, Minet O, Helfmann J, Herrig M, Muller G 1996. The spatial variation of the refractive index in biological cells. Phys Med Biol 41(3):369-382.
18. Wang C, Zhong X, Ruffner DB, Stutt A, Philips LA, Ward MD, Grier DG 2016. Holographic Characterization of Protein Aggregates. J Pharm Sci 105(3):1074-1085.
19. Cavicchi RE, King J, Ripple DC 2018. Measurement of Average Aggregate Density by Sedimentation and Brownian Motion Analysis. J Pharm Sci 107(5):1304-1312.
20. Gardiner C, Shaw M, Hole P, Smith J, Tannetta D, Redman CW, Sargent IL 2014. Measurement of refractive index by nanoparticle tracking analysis reveals heterogeneity in extracellular vesicles. J Extracell Vesicles 3:25361.
21. Leviton DB, Frey BJ 2006. Temperature-dependent absolute refractive index measurements of synthetic fused silica. Proc Spie 6273.
22. Malitson IH 1965. Interspecimen Comparison of the Refractive Index of Fused Silica. J Opt Soc Am 55(10):1205-1209.
23. Van der Pol E, Van Gemert MJC, Sturk A, Nieuwland R, Van Leeuwen TG 2012. Single vs. swarm detection of microparticles and exosomes by flow cytometry. Journal of Thrombosis and Haemostasis 10(5):919-930.

24. Parida BK, Garrastazu H, Aden JK, Cap AP, McFaul SJ 2015. Silica microspheres are superior to polystyrene for microvesicle analysis by flow cytometry. Thromb Res 135(5):1000-1006.
25. Zhang WQ, Tian Y, Hu XX, He SB, Niu Q, Chen CX, Zhu SB, Yan XM 2018. Light-Scattering Sizing of Single Submicron Particles by High-Sensitivity Flow Cytometry. Anal Chem 90(21):12768-12775.
26. Welsh JA, Horak P, Wilkinson JS, Ford VJ, Jones JC, Smith D, Holloway JA, Englyst NA 2020. FCMPASS Software Aids Extracellular Vesicle Light Scatter Standardization. Cytom Part A 97(6):569-581.
27. de Rond L, Coumans FAW, Nieuwland R, van Leeuwen TG, van der Pol E 2018. Deriving Extracellular Vesicle Size From Scatter Intensities Measured by Flow Cytometry. Curr Protoc Cytom 86(1):e43.
28. Varga Z, Van Der Pol E, Palmai M, Garcia-Diez R, Gollwitzer C, Krumrey M, Fraikin JL, Gasecka A, Hajji N, Van Leeuwen TG, Nieuwland R 2018. Hollow organosilica beads as reference particles for optical detection of extracellular vesicles. Journal of Thrombosis and Haemostasis 16(8):1646-1655.
29. Wang L, Hoffman RA. 2017. Flow Cytometer Performance Characterization, Standardization, and Control. In Robinson JP, Cossarizza A, editors. Single Cell Analysis: Contemporary Research and Clinical Applications, ed., Singapore: Springer Singapore. p 171-199.
30. Mie G 1908. Considerations on the optics of turbid media, especially colloidal metal solutions. Ann Phys 25:377-442.
31. Hulst HC, van de Hulst HC. 1981. Light scattering by small particles. ed.: Courier Corporation.
32. Roßkamp D, Truffer F, Bolay S, Geiser M 2007. Forward scattering measurement device with a high angular resolution. Optics express 15(5):2683-2690.
33. Doornbos RM, Hoekstra AG, Deurloo KE, De Grooth BG, Sloot PM, Greve J 1994. Lissajous-like patterns in scatter plots of calibration beads. Cytometry 16(3):236-242.
34. Satinover SJ, Dove JD, Borden MA 2014. Single-particle optical sizing of microbubbles. Ultrasound Med Biol 40(1):138-147.
35. Fattaccioli J, Baudry J, Emerard JD, Bertrand E, Goubault C, Henry N, Bibette J 2009. Size and fluorescence measurements of individual droplets by flow cytometry. Soft Matter 5(11):2232-2238.
36. Welsh JA, Jones JC 2020. Small Particle Fluorescence and Light Scatter Calibration Using FCM(PASS) Software. Curr Protoc Cytom 94(1):e79.
37. Certain commercial instruments are identified to adequately specify the experimental procedure. In no case does such identification imply endorsement by the National Institute of Standards and Technology.
38. Vandesteeg N, Kilbert C 2013. Differentiation of subvisible silicone oil droplets from irregular standard dust particles. J Pharm Sci 102(6):1696-1700.
39. Verkouteren JR, Leigh SD 2000. New low-index liquid refractive index standard: SRM 1922. Fresenius J Anal Chem 367(3):226-231.
40. Ripple DC, Hu ZS 2016. Correcting the Relative Bias of Light Obscuration and Flow Imaging Particle Counters. Pharm Res 33(3):653-672.
41. He J, Liu W, Huang YX 2016. Simultaneous Determination of Glass Transition Temperatures of Several Polymers. Plos One 11(3).
42. Homola J. 2006. Surface plasmon resonance based sensors. ed.: Springer.
43. Morris TA, Peterson AW, Tarlov MJ 2009. Selective binding of RNase B glycoforms by polydopamine-immobilized concanavalin A. Anal Chem 81(13):5413-5420.
44. Grassi JH, Georgiadis RM 1999. Temperature-dependent refractive index determination from critical angle measurements: Implications for quantitative SPR sensing. Anal Chem 71(19):4392-4396.
45. 2017. SCHOTT Zemax catalog ed.
46. Daimon M, Masumura A 2007. Measurement of the refractive index of distilled water from the near-infrared region to the ultraviolet region. Appl Opt 46(18):3811-3820.

47. Kozma IZ, Krok P, Riedle E 2005. Direct measurement of the group-velocity mismatch and derivation of the refractive-index dispersion for a variety of solvents in the ultraviolet. J Opt Soc Am B 22(7):1479-1485.
48. Moutzouris K, Papamichael M, Betsis SC, Stavrakas I, Hloupis G, Triantis D 2014. Refractive, dispersive and thermo-optic properties of twelve organic solvents in the visible and near-infrared. Appl Phys B-Lasers O 116(3):617-622.
49. Jenkins FA, White HE. 1976. Fundamentals of optics. 4th ed., New York: McGraw-Hill.
50. Welsh JA, Jones JC, Tang VA 2020. Fluorescence and Light Scatter Calibration Allow Comparisons of Small Particle Data in Standard Units across Different Flow Cytometry Platforms and Detector Settings. Cytom Part A 97(6):592-601.
51. Maltseva M, Langlois MA 2022. Flow Virometry for Characterizing the Size, Concentration, and Surface Antigens of Viruses. Curr Protoc 2(2):e368.
52. van der Pol E, van Leeuwen TG, Yan XM 2021. Misinterpretation of solid sphere equivalent refractive index measurements and smallest detectable diameters of extracellular vesicles by flow cytometry. Sci Rep-Uk 11(1).
53. Laven P 2006. MiePlot. URL: http://philiplaven com/mieplot htm(visited on 8/26/2022).
54. Zhuang ZW, He C, Du Y, Wen WH, Zhang GL, Zhao YQ, Tao M, Hu ZL, Wang K, Qiu P 2019. Refractive index and pulse broadening characterization using oil immersion and its influence on three-photon microscopy excited at the 1700-nm window. J Biophotonics 12(2).

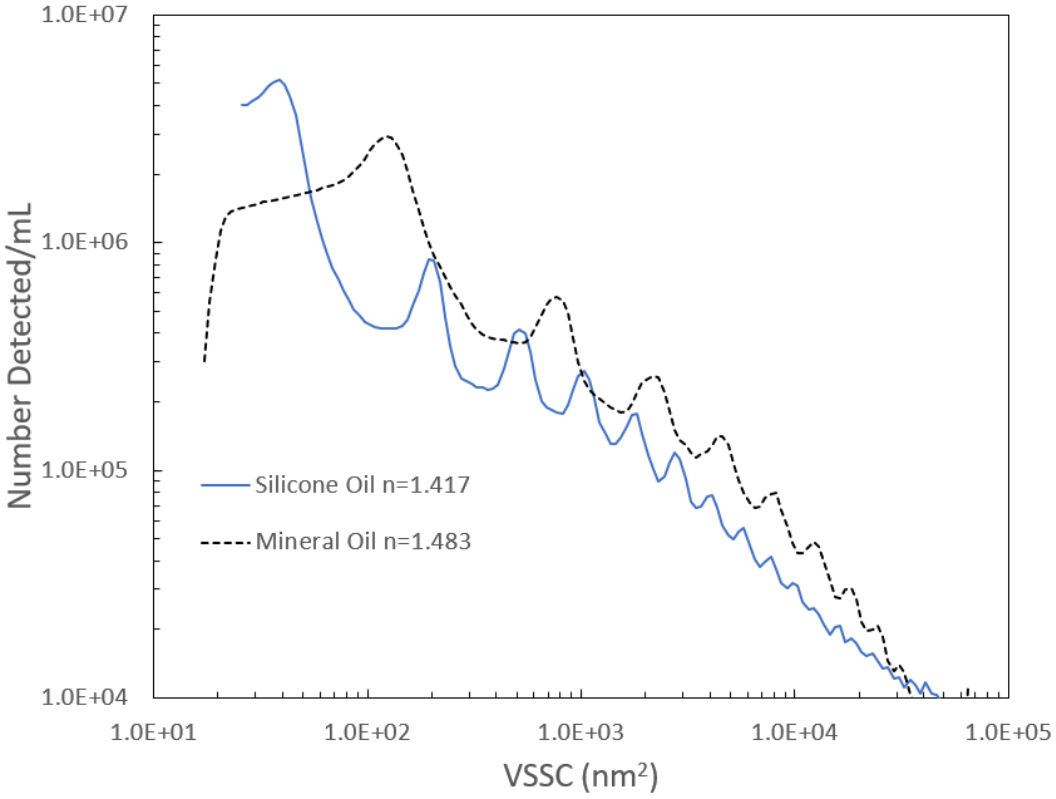

Figure 1. Histogram of particles detected at 405 nm (VSSC) for samples containing silicone oil droplets (solid blue line) and mineral oil droplets (dashed line).

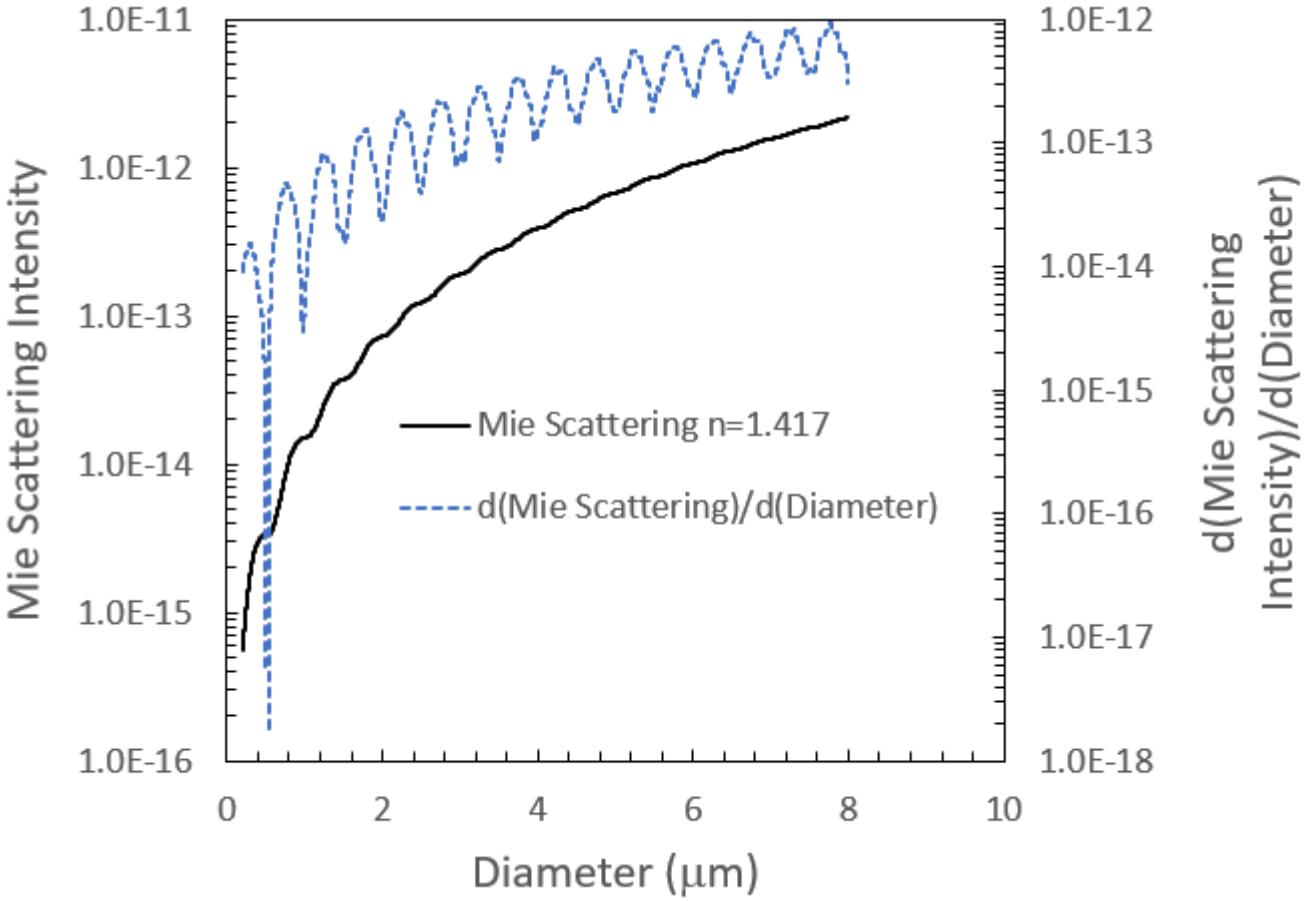

Figure 2. Calculated (using Mieplot) scattering intensity vs diameter for a sphere with n=1.417 in water (solid black, left-axis) and the derivative (d(Mie Scattering signal)/d(Diameter) (dashed blue, right-axis). Approximate period is 0.5 μm.

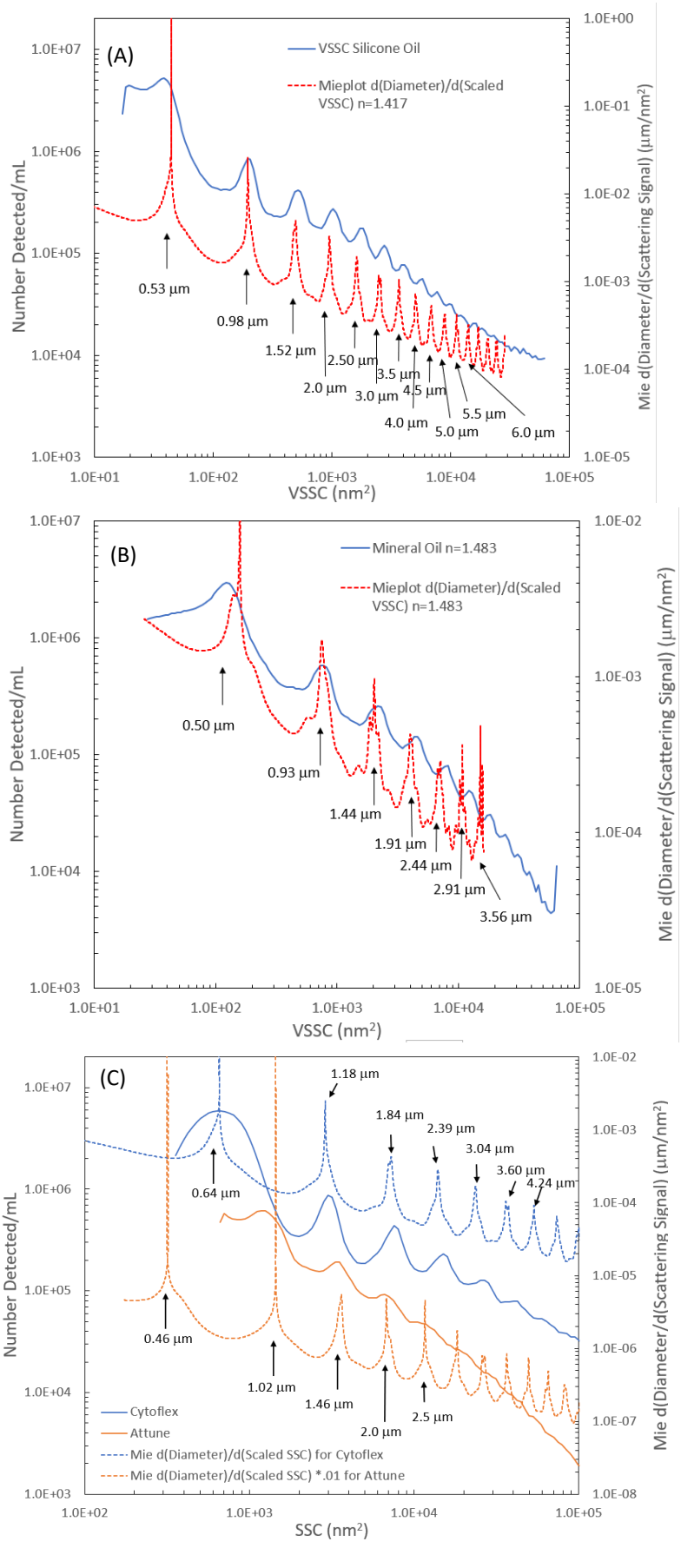

Figure 3. (A) Histogram of particles detected at 405 nm (VSSC) for samples containing silicone oil droplets (solid blue line, left axis) and the derivative vs VSSC d(Diameter)/d(Mie Scattering signal) (dashed red line, right axis), where the calculated scattering intensity is scaled using results from 1.2 µm silica microspheres. Diameters indicated by the arrows come from the corresponding diameter from the Mie calculation. (B) Histogram of particles detected at 405 nm (VSSC) for samples containing mineral oil droplets (solid blue line, left axis) and the derivative d(Diameter)/d(Mie Scattering signal) vs VSSC (dashed red line, right axis). (C) Histogram of particles detected at 488 nm (SSC) for samples containing silicone oil droplets (solid line, left axis) and the derivative vs SSC d(Diameter)/d(Mie Scattering signal) (dashed line, right axis). Blue curves correspond to results and modeling for Cytoflex instrument, and Orange for the Attune NXT. Modeling data for the latter is scaled by 0.01 for clarity. For the Cytoflex, approximate period is 0.6 µm, contrasting with the period 0.5 µm for the data at 405 nm (A).

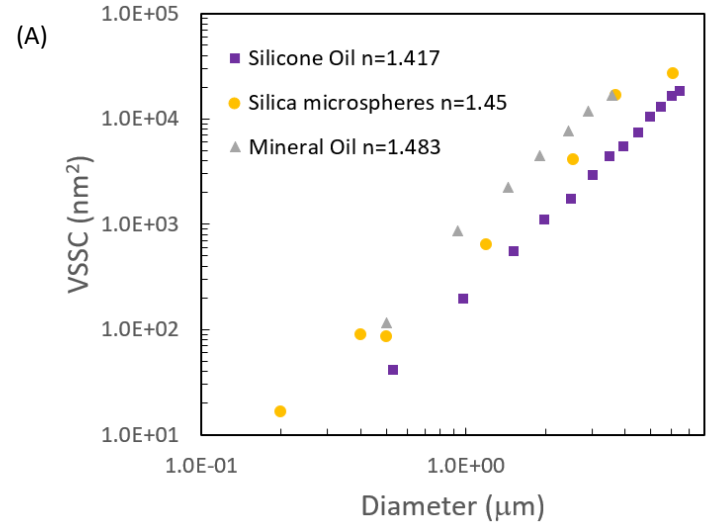

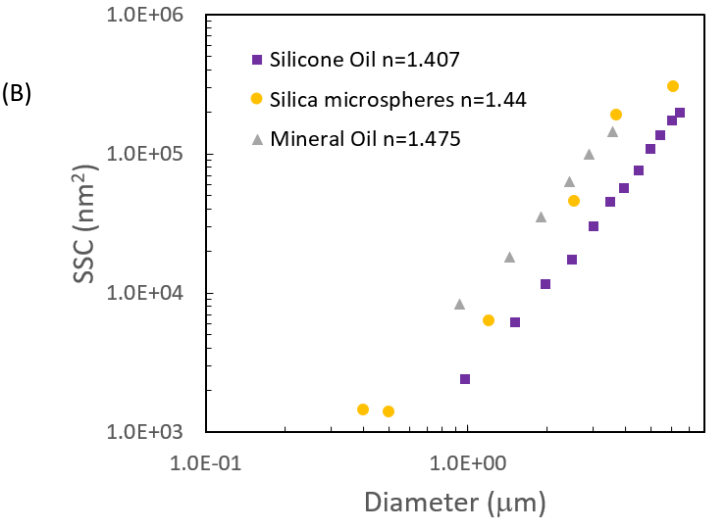

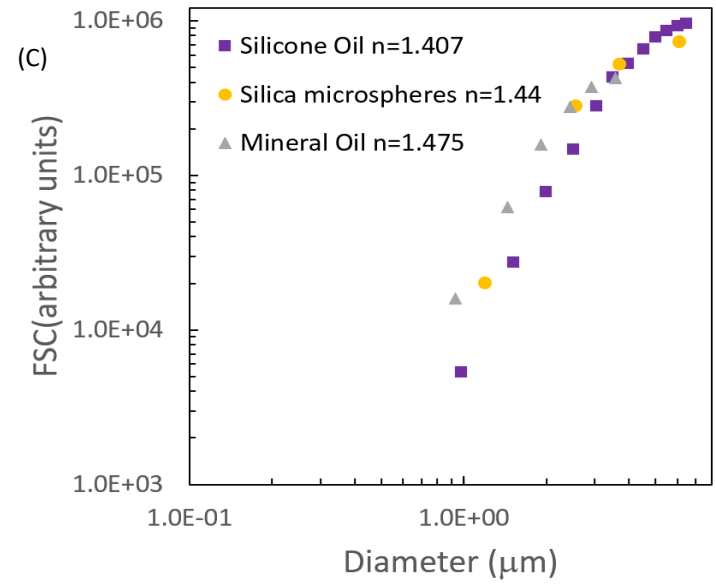

Figure 4. Scattering intensity vs particle diameter for droplets of silicone oil (purple squares) and mineral oil (gray triangles) in water and silica microspheres for (A) VSSC, (B) SSC, and (C) FSC.

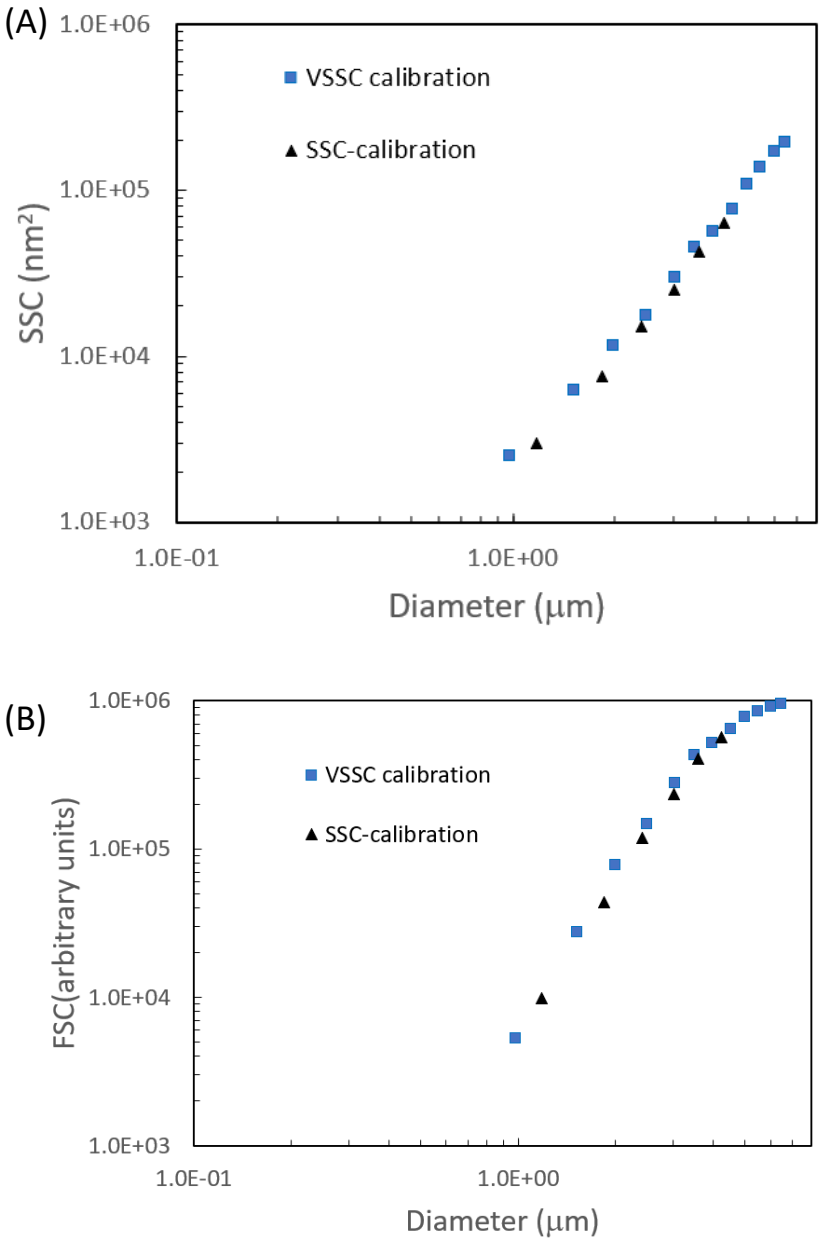

Figure 5. Comparison of silicone oil droplet results where calibration was performed using the VSSC data (blue squares) and SSC data (black triangles) for (A) SSC and (B) FSC.

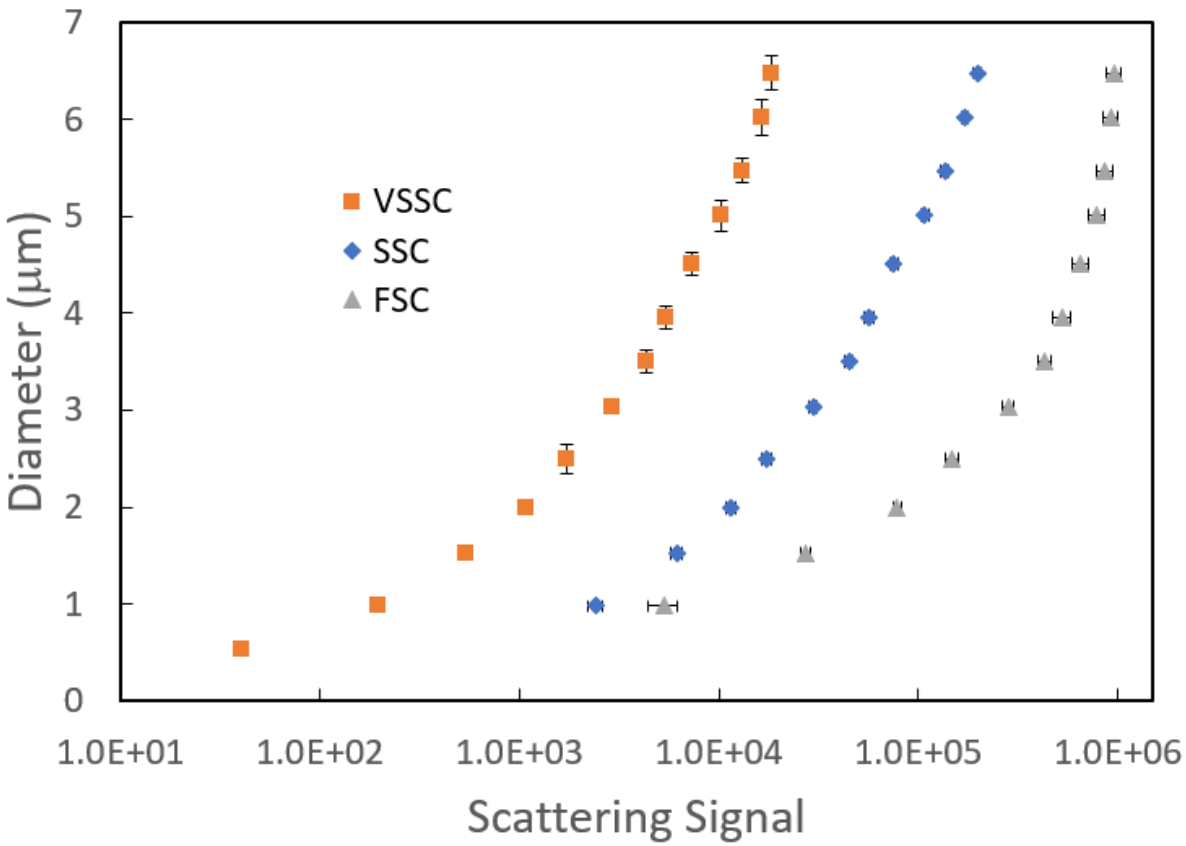

Figure 6. Silicone oil droplet diameter vs scattering signal for VSSC (orange squares), SSC (blue diamonds), and FSC (gray triangles). Vertical error bars appearing on some of the VSSC data points (for some, the error bars are smaller than the symbol) represent the spread in diameter assignments as illustrated in Supplementary Figure 8 due to possible error in *n* or collection angle. Uncertainty in the scattering signal for VSSC data points from the standard deviation from measurements made at different dates (Supplementary Figure 5) ranged from one to four percent of the scattering signal value and were smaller than the size of the data points. Error bars on the SSC and FSC represent the standard deviation in SSC and FSC values obtained from VSSC data points that have a scattering signal within two percent of the plotted VSSC points. This represents expected scatter in FSC and SSC among individual points and includes effects of the higher noise in those channels. The data points themselves for SSC and FSC represent the mean value, for which an error bar would be the standard error of the mean, which is less than one percent of the scattering value and smaller than the data points. Scattering signal is in SCS units (nm^2) for VSSC and SSC, and in the arbitrary units reported by the instrument for FSC.

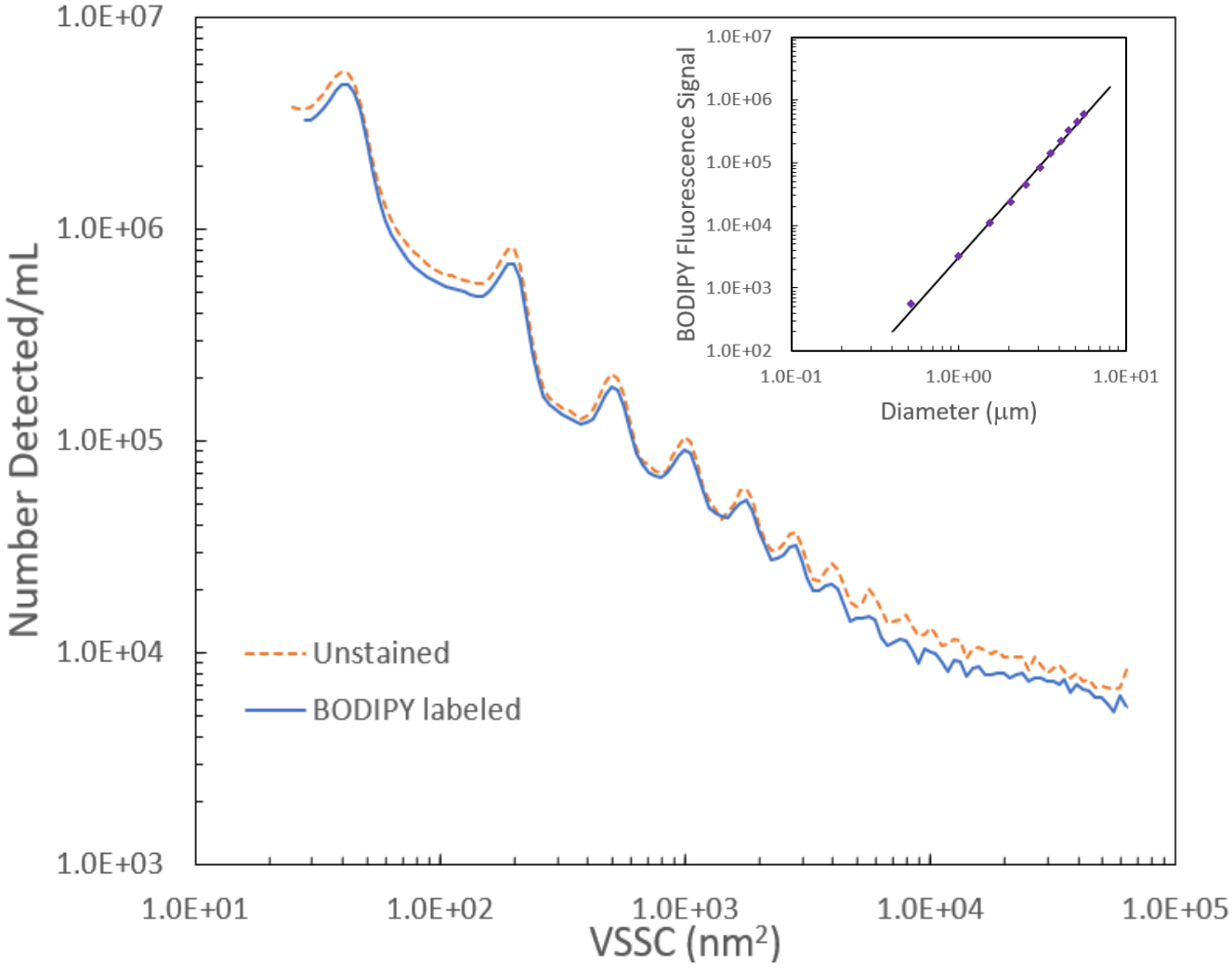

Figure 7. BODIPY-stained silicone oil droplets (solid orange line) and unstained droplets (dashed blue line). Inset: Bodipy fluorescence signal vs silicone oil droplet diameter as calibrated by Mie resonance, (purple diamond), and fit of fluorescence signal to the cube of the diameter.